We are IntechOpen, the world's leading publisher of Open Access books Built by scientists, for scientists

4,800
Open access books available

122,000
International authors and editors

135M
Downloads

Our authors are among the

154
Countries delivered to

TOP 1%
most cited scientists

12.2%
Contributors from top 500 universities

WEB OF SCIENCE™

Selection of our books indexed in the Book Citation Index in Web of Science™ Core Collection (BKCI)

Interested in publishing with us?
Contact book.department@intechopen.com

Numbers displayed above are based on latest data collected.
For more information visit www.intechopen.com

23

Nonlinear Waves in Transmission Lines Periodically Loaded with Tunneling Diodes

Koichi Narahara
Yamagata University
Japan

1. Introduction

We review the properties of nonlinear waves on the electrical transmission lines periodically loaded with tunneling diodes (TDs) termed—TD lines.In general, the transmission equation of a linear dispersive line allows both sinusoidal and exponential solutions. However, exponential solutions are usually discarded because they diverge at infinity, and therefore, do not satisfy any physically meaningful boundary conditions. In a TD line, once the input pulse crosses the peak voltage of the loaded TDs, the exponential wave develops atsmaller voltagesthan the peak, and the ordinary sinusoidal wave is coupled to it atgreater voltages. The sinusoidal part can continuously unite with the leading exponential wave, so that the exponential wave can be formed along the dispersive line without violating physical boundary conditions. By developing exponential waves, a TD line exhibits technologically useful properties that result in the generation and management of short pulses.When an impulse is input to a TD line, the resulting exponential wave is much steeper than the input; therefore, the input pulse experiences significant shortening.
Moreover, when a rising step pulse, whose bottom and top voltage levels lie in the voltage ranges below and above the peak voltage is input, the pulse edge oscillates on the line.
This chapter discusses nonlinear wave propagation on TD lines in detail. We first define TD lines and describes their circuit configuration and principle of operation. We employ an idealized model of a TD line, which makes a comprehensive description of the operating principles possible. It also gives us design criteria for a short-pulse generator or oscillator using TD lines. We then examine the validity of the analytically obtained design criteria through numerical integration of the transmission equations of a TD line. We alsocharacterize the line using full-wave calculations for monolithically integrated lines. Next, severalexperimental results are described, which are obtained by the time-domain measurements using TD lines breadboarded with Esaki diodes. Finally, we describe the potential of TD lines for the management of short pulses.

2. Fundamentals of TD lines

Figure 1(a) shows a circuit diagram of a TD line, where L, R, C, and G represent the series inductor, series resistor, shunt capacitor, and shunt TD of the unit cell, respectively. The typical current-voltage relationshipof a TD is shown by the dotted curve in Fig. 1(b). For simplicity, we idealize it as the solid curve in Fig. 1(b) (Richer, 1966). The voltage levels

Source: Wave Propagation in Materials for Modern Applications, Book edited by: Andrey Petrin,
ISBN 978-953-7619-65-7, pp. 526, January 2010, INTECH, Croatia, downloaded from SCIYO.COM

where TDs exhibit a negative differential resistance (NDR) degenerate to a threshold V_{pk} and the finite conductance above V_{pk} is neglected. We can then write the current through TDs as $G = G_0\theta(V_{pk}-V)$, where $\theta(V)$ shows the Heaviside function. Hereafter, we consider the situations where an impulse or a step pulse is input to the line, such that they cross V_{pk}. Figure 2 shows the signal applications. For convenience, we call the voltage range greater (less) than V_{pk} regions I(II). The present simplified TD model shows that the pulse is influenced by finite shunt conductance in region II and is completely loss free in region I.

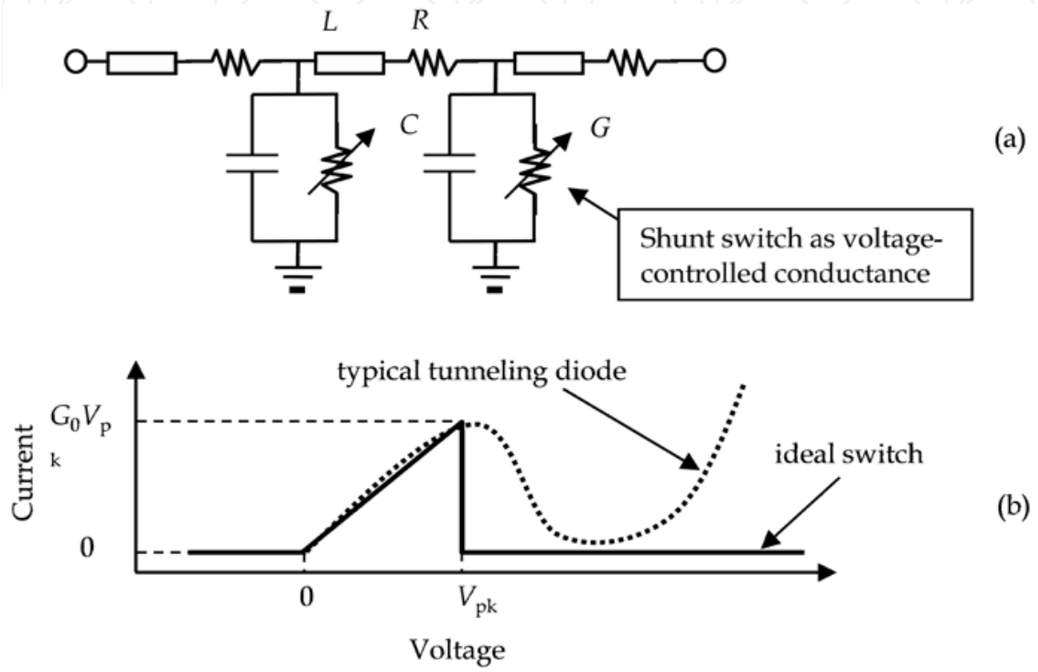

Fig. 1. Circuit configuration of TD lines. (a) The unit cell of TD lines and (b) current-voltage relationship of TDs.

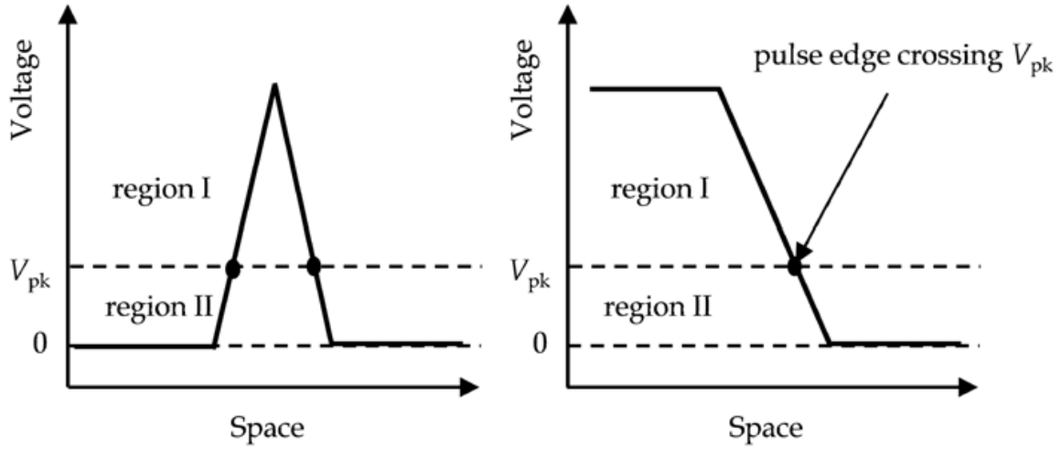

Fig. 2. Signal applications.

When denoting the voltage and current at the nth node as V_n and I_n, respectively, the transmission equation of the line is given by

$$l\frac{dI_n}{dt} = \frac{V_n - V_{n+1}}{d} - rI_n, \tag{1}$$

$$c\frac{dV_n}{dt} = \frac{I_{n-1} - I_n}{d} - gV_n, \tag{2}$$

where d is the length of the unit cell. Moreover, $l = L/d$, $c = C/d$, $r = R/d$, and $g = G_0/d$ are the series inductance per unit length, shunt capacitance per unit length, and shunt conductance per unit length, respectively.The line is linear and dispersive when considering only regions I and II. Thus, it is meaningful to analyze the dispersion curves in each region. The phase velocities normalized by $1/(lc)^{0.5}$ of the modes having wave number k are explicitly given by

$$v_{I,\sin} = \frac{1}{2kd}\sqrt{-\alpha^2 + 16\sin^2\frac{kd}{2}}, \tag{3}$$

$$v_{I,\exp} = \frac{1}{2kd}\left(-\alpha + \sqrt{\alpha^2 + 16\sinh^2\frac{kd}{2}}\right), \tag{4}$$

$$v_{II,\exp} = \frac{1}{2kd}\left(-\alpha - \beta + \sqrt{(\alpha-\beta)^2 + 16\sinh^2\frac{kd}{2}}\right), \tag{5}$$

where $v_{\mathrm{I,sin}}$, $v_{\mathrm{I,exp}}$, and $v_{\mathrm{II,exp}}$ show the normalized phase velocities of the sinusoidal mode in region I, the exponential mode in region I, and the exponential mode in region II, respectively. Moreover, α and β are normalized series resistance and shunt conductance given by

$$\alpha = rd\sqrt{\frac{c}{l}}, \tag{6}$$

$$\beta = gd\sqrt{\frac{l}{c}}. \tag{7}$$

We employ the sign convention: $\omega t - nkd$for positive propagation. Thus, in region I, $k$must be negative, while in region II, it must be positive for exponential modes.

Figure 3 shows the dispersion curves for α=0.18 and β=2.0. The horizontal axis shows the wave number with a unit of the inverse of d, and the vertical axis shows the normalized phase velocities. For steady or quasisteady pulse propagation, the velocity of the pulse edge in region I must be the same as that in region II. When the pulse propagates forward, the exponential mode in region II can only couple with the sinusoidal mode in region I because no exponential counterpart is present. At point P, the velocity and steepness are coincident, so that the forward pulse occupies the region around this point in Fig. 3. Note that the wavenumber at P is relatively large, so that for the forward-propagating pulse, short-wavelength oscillatory waves should be observed in region I, which is supported by an exponential wave developed in region II. According to this mechanism, when an impulse is applied to the TD line, it finally reaches the cross-point of $v_{\mathrm{I,sin}}$ and $v_{\mathrm{II,exp}}$. Initially, a wave

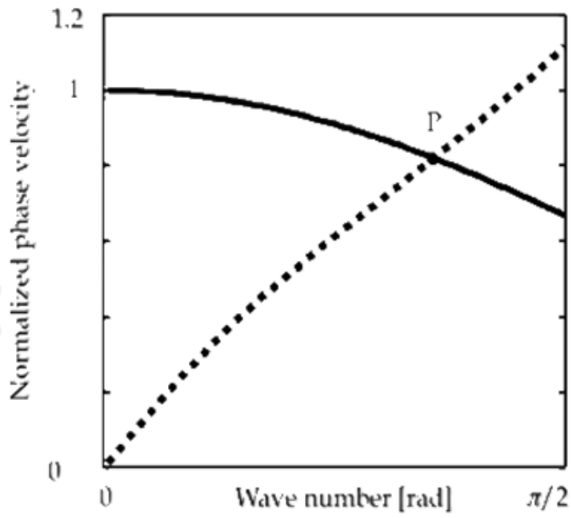

Fig. 3. Dispersion of TD line. The solid and dotted curves represent the normalized velocities in regions I and II, respectively.

component of an input pulse having a specific wave number must have different velocities between region I and region II. Thus, for coincidence of the velocities in both the regions I and II, the wave component experiences a wavelength shortening. As a result, the width of the incident pulse is greatly reduced (Narahara et al., 2005). Because the wave number at the cross point of the curves $v_{I,sin}$ and $v_{II,exp}$ becomes larger for greater β, the greater the conductance, the more the pulse is shortened.

Similar pulse shortening is possible in Schottky-contacted TD lines. It is well known that a Schottky-contacted line exhibits several useful properties for high-speed electronics (Scott, 1970). When a pulse is input such that the nonlinearity of the Schottky varactors compensates for dispersion, the line generates multiple solitonic pulses, whose widths are generally smaller than that of the input. By extracting the largest pulse, a Schottky-contacted line operates as a good short pulse generator (Kintis et al., 2008). Moreover, when a step pulse is input such that both the nonlinearity and dispersion sharpen the edge, the edge finally results in a shock, by which a sub-picosecond temporal transient is observed (Rodwell et al., 1994). It is found that the larger soliton travels more than the smaller one in Schottky-contacted TD lines; therefore, we obtain highly shortened pulse by detecting only the largest soliton (Narahara et al., 2006).

On the other hand, when a step pulse is applied to the line, the pulse edge oscillates, as shown in Fig. 4. The spatial position on the line is shown horizontally, and the voltage is shown vertically. Figure 4(a) shows the behavior of the forward pulse. Because the forward pulse, combining a sinusoidal mode in region I and an exponential mode in region II, does not have permanent profile, it is not stable—it becomes attenuated and finally disappears, leaving only the exponential pulse edge is in region II, as shown in Fig. 4(b). This edge develops exponential modes in region I to form a stable pulse, and then starts traveling backward, as shown in Fig. 4(c). When the backward stable pulse reaches the input, it is reflected as in Fig. 4(d), and again begins to travel forward as an unstable sinusoidal-exponential wave (Narahara, 2006). This process continues permanently with proper boundary condition.

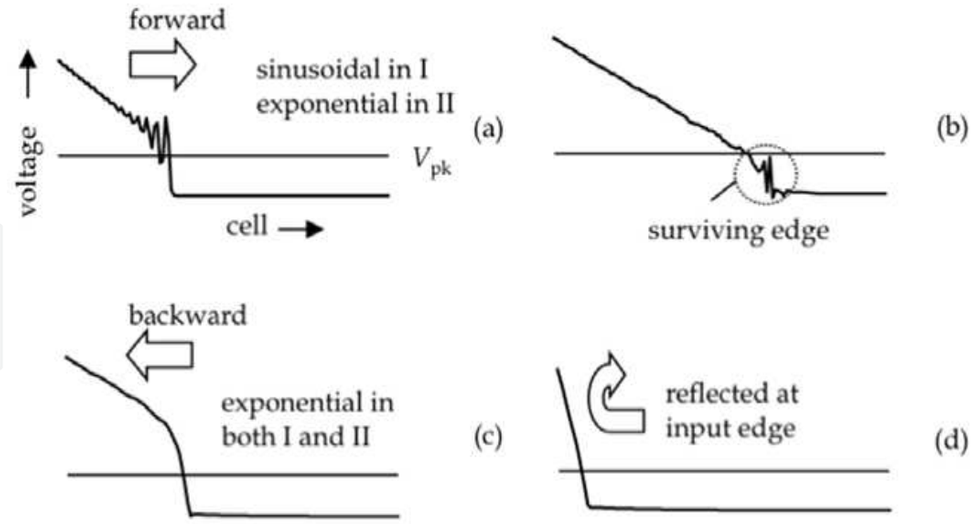

Fig. 4. Step pulse in TD line.

3. Numerical characterization of TD lines

3.1 Transmission line analysis

To validate the above given qualitative discussion and to observe the pulse shortening, we numerically solved Eqs.(1) and (2). Figure 5 shows the typical behavior of a pulse propagating along a TD line. We set c, l, V_{pk}, β, and d to 6.0 pF/mm, 3.0 nH/mm, 0.2 V, 0.75, and 50 μm, respectively. For the present parameters, the phase velocity at a long wavelength is 0.025 c_0 (c_0: the velocity of light in vacuum) and the cutoff frequency is 47.5 GHz.

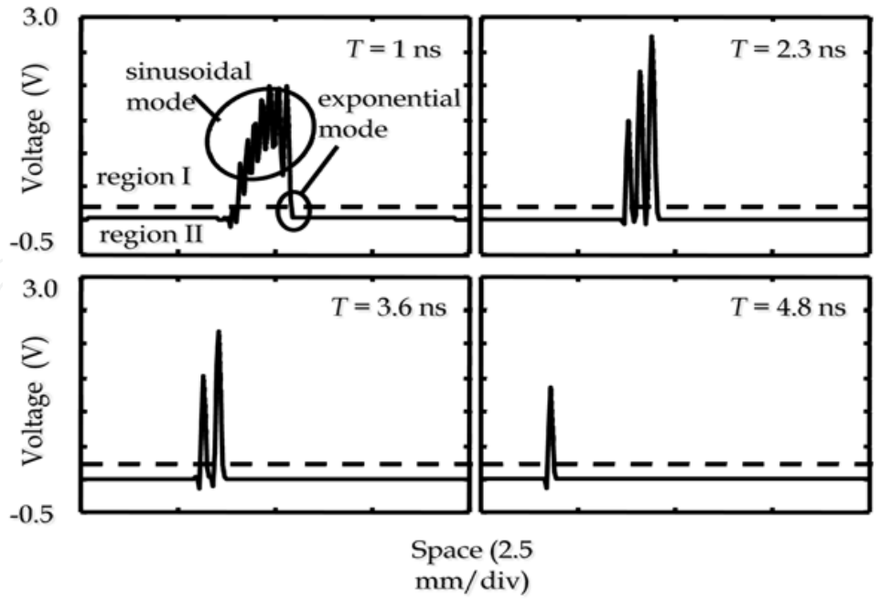

Fig. 5. Impulse in TD line.

Input, an impulse of a Gaussian form with an amplitude of 1.5 V and a full-width at half-maximum (FWHM) of 100.0 ps is supplied. The waveforms at 1.0, 2.3, 3.6 and 4.8 ns after the

Gaussian impulse starts to be input are shown in Fig. 5. Oscillation, which is caused by the development of the sinusoidal wave in region I, is observed at every temporal point. Moreover, the wave number of the oscillation decreases as time progresses. Finally, the sinusoidal wave in region I becomes monocycled at 4.8 ns, so that the waveform becomes a single short pulse, whose FWHM is estimated to be 12.5 ps.

Figure 6 shows the behavior of a propagating step pulse. We set c, l, V_{pk}, α, β, and d to 6.0 pF/mm, 3.0 nH/mm, 0.2 V, 0.02, 2.0, and 50 μm, respectively. The waveforms on a switch line after an elapse of every hundred picoseconds are shown sequentially from top to bottom in Fig. 6. For forward pulses, which moves toward the output as specified by S_F in Fig.6, the pulse exhibits eminent oscillatory behavior in region I, which proves the development of the sinusoidal wave in region I. Moreover, the pulse is gradually attenuated and disappears at around point P in Fig.6. Then, the pulse starts to propagate backward, as shown by S_B in Fig.6. For the pulses in S_B, no oscillatory behavior is observed, unlike the

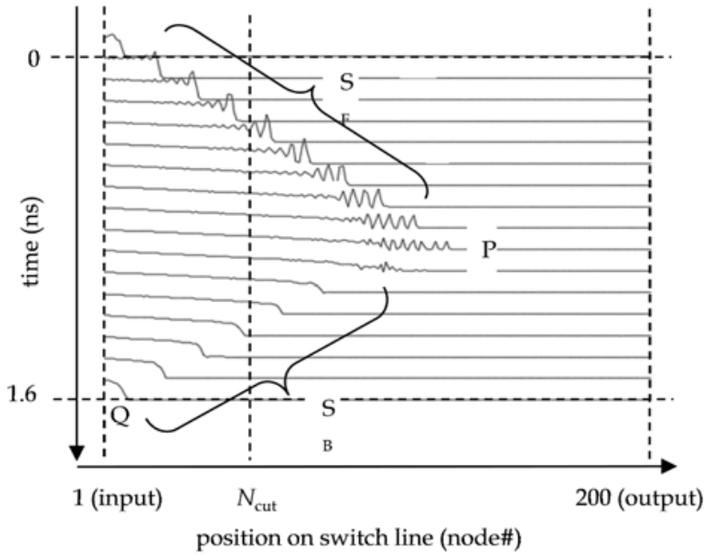

Fig. 6. Numerically obtained step pulse response of TD line.

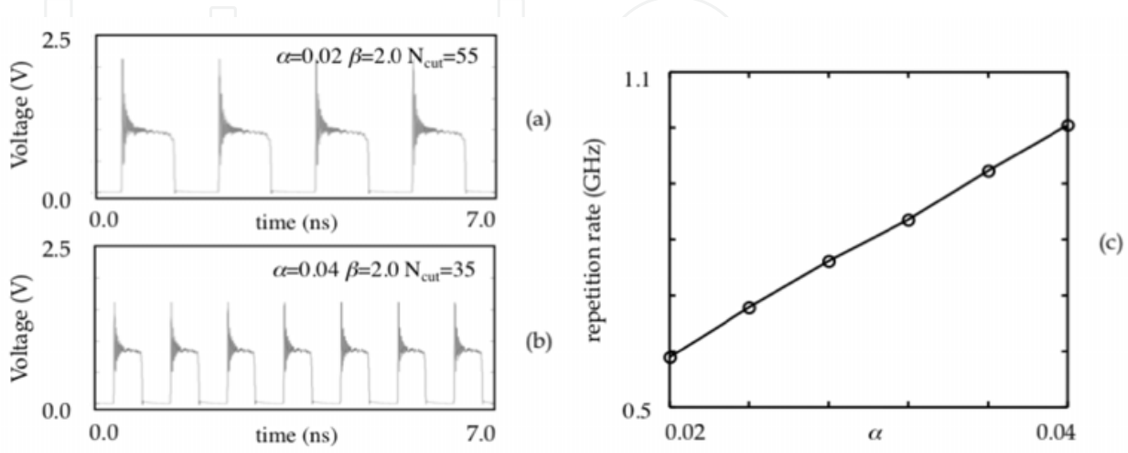

Fig. 7. Dependence of edge's oscillating period on normalized resistance α.

pulses in S_F. This observation results from the fact that exponential waves develop in both regions I and II and establish a stable propagation. The backward pulse reaches the input edge at Q in Fig.6 and then is reflected to start forward propagation again in quasisteady manner. The oscillating pulse edge is numerically confirmed. To see this more clearly, the seven-nanosecond slice at node N_{cut} in Fig.6 is shown in Fig. 7. Figures 7(a) and (b) show the temporal variations of the pulse voltage at N_{cut}=55 on a TD line with α=0.02 and at N_{cut} =35 with α=0.04, respectively. Both exhibit periodic pulse trains, indicating that the pulse edge oscillates. Present calculations simulate the case where the voltage source is directly coupled with a TD line, so that the input port of the line functions as a fixed-value boundary for the traveling pulses. Thus, in the calculations, the backward pulse is totally reflected at the input port, so that the back-and-forth edge motion continues permanently. Practically, the design of the interconnection between the pulse source and a switch line is very important to guarantee permanent oscillation. It is interesting to note that the repetition rate increases when α increases. Figure 7(c) shows this dependence. The repetition rate is vertically plotted for six different values of α. The repetition rate increases proportionally with increasing α. This is because the increase in α contributes to the decrease in the round-trip distance. Increases in β and V_{pk} have the same effect. Moreover, when the amplitude of the input pulse increases, the round-trip time becomes longer, reducing the oscillation frequency. By this simple arrangement, the device can act as a voltage-controlled oscillator. By proper design of loss elements such as electrode loss, switch conductance, and signal application, we can obtain an oscillator having the required oscillation frequency (Narahara, 2006).

3.2 Full-wave analysis

Above all, resonant tunneling diodes (RTDs) exhibit the most excellent performance in submillimeter and terahertz bands (Brown et al., 1991, Ohashi et al., 2005). To design monolithically integrated RTD lines, a full-wave solver of Maxwell's equations must be required.Afinite-difference time-domain (FDTD) method (Taflove, 1995) best suits to the present purpose. In an FDTD, a circuit element such as a capacitor, an inductor, and anonlinear device, are usually implemented as field-dependent conductance and capacitance in a single Yee cell (Yee, 1966). For example, when the conduction current density flowing in the device is denoted by $\vec{J}_L$, the temporal evolution of the electromagnetic fields is calculated on the basis of an extended Ampere's law as

$$\varepsilon \frac{\partial \vec{E}}{\partial t} = \vec{\nabla} \times \vec{H} - \vec{J}_L, \tag{8}$$

where $\vec{E}$, $\vec{H}$, and ε are the electric field, magnetic field, and dielectric constant, respectively. By the single-cell implementation of the lumped device, Eq. (8) is converted as follows:

$$E_z^n = E_z^{n-1} + \frac{\Delta t}{\varepsilon}\left(\vec{\nabla} \times \vec{H}^{n-1/2}\right)_z - \frac{\Delta t}{\Delta y \, \Delta x} {I_{L,z}}^{n-1/2}, \tag{9}$$

where Δx, Δy, and Δt show the cell size in the x, y, and t directions, respectively. The superscripts show the temporal positions, by which we represent the alternative evaluations of electrical and magnetic fields in FDTD, and $\vec{I}_L$ shows the device current, which is

assumed to flow in the z direction, and is equal to $J_L \Delta x\, \Delta y$. Moreover, when $\vec{I}_L$ depends on the terminal voltage, $\vec{I}_L$ becomes a function of $E_z \Delta z$ at the corresponding cell. Note that the argument of $\vec{I}_L$ is evaluated at time n for numerical stability (Luebbers et al., 1993); therefore, we need root-finding routines such as the Newton–Raphson method, to obtain the temporal advanced electrical fields. The situations are more complicated when the device size is significant compared with that of the circuit. When a device occupies N adjacent cells, the difference equations to be solved become

$$E_z^n[i] = E_z^{n-1}[i] + \frac{\Delta t}{\varepsilon}\left(\vec{\nabla} \times \vec{H}^{n-1/2}[i]\right)_z - \frac{\Delta t}{\Delta y\, \Delta x} I_{L,z}{}^{n-1/2}\left(E_z^n[1], E_z^n[2], \cdots, E_z^n[N]\right), \tag{10}$$

where $X[i]$ (X=E_z, H) represents the field at the ith cell occupied by the device. For the present case, we have to find roots of a multiple-variable function. This root-finding procedure is very time consuming, whereas the analysis of a TD line needs many distributed TD models; therefore, some simplification is unavoidable. To eliminate the performance-limiting root-finding procedures, we approximate the voltage dependence of the device current by a piecewise-linear (PWL) function (Narahara et al., 2008a). The key is the fact that $E_z^n[i]$ is solved by hand in Eq. (10), when $\vec{I}_L{}^{n-1/2}$ is a linear function of the arguments.When we put I_j=$I_L(V_j)$ for Mdifferent voltages V_j, as shown in Fig.8, I_L is approximated by the following PWL function:

$$I_L(V) = \frac{I_{j+1} - I_j}{V_{j+1} - V_j}(V - V_j) + I_j, \tag{11}$$

for V_j<V<V_{j+1}. Substituting I_L from Eq. (10), we obtain

$$\mathbf{E}_z{}^n = \mathbf{A}[j]^{-1}\mathbf{S}[j], \tag{12}$$

where $\mathbf{E}_z{}^n$ shows the column vector $(E_z{}^n[1], E_z{}^n[2], \cdots, E_z{}^n[N])^t$ and

$$\mathbf{A}[j]_{kl} = \delta_{kl} + \frac{\Delta t\, \Delta z}{\varepsilon\, \Delta x\, \Delta y}\frac{I_{j+1} - I_j}{V_{j+1} - V_j}, \tag{13}$$

$$\mathbf{S}[j]_k = E_z{}^{n-1}[k] + \frac{\Delta t}{\varepsilon}(\vec{\nabla} \times \vec{H}[k])_z - \frac{\Delta t}{\varepsilon \Delta x \Delta y}\frac{I_j V_{j+1} - I_{j+1} V_j}{V_{j+1} - V_j}, . \tag{14}$$

$\mathbf{A}[j]_{kl}$ (k,l=1,2,...,N) and $\mathbf{S}[j]_k$ (k=1,2,...,N) show the (k,l)th entry of $\mathbf{A}[j]$, and the kth component of $\mathbf{S}[j]$, respectively. After obtaining $E_z{}^n[i]$ using Eq.(12), we have to check if the terminal voltage V is really in the range V_j<V<V_{j+1} with $V = \Delta z \sum_{i=1}^{N} E_z{}^n[i]$. If not, the procedure is repeated with other$j$ values, until $V$is within (V_j,V_{j+1}).

In the following, we show the results of a sample three-dimensional FDTD calculations that demonstrateoscillating pulse edge along aTD line. The calculation setup is illustrated in Fig.9. Based on a coplanar waveguide, TDs are placed every 30 μm beneath the signal line. The total cell size is 100×100×100 and the spatial increments $\Delta x, \Delta y, \Delta z$ are all set to 10 μm. Each TD is represented by a singleE_z node. We simplify the TD current as a PWL function with M=27 to model an InP-based RTD (Sugiyama, 1995). V_1 (V_{27}) is taken to be sufficiently

small (large) for the inclusion of any voltages needed for the calculations. The peak and valley voltages are set to 0.4 and 0.45 V, respectively. The input is a step pulse with amplitude 1.5 V and a 5 ps rise time. The pulse edge achieves steady oscillation with a period of about 3.8 ps. Figure 10 shows this steady oscillation of the edge. The spatial variations of line voltage are plotted and recorded at 0.38 ps intervals. The FDTD calculation successfully demonstrates the potential of monolithically integrated TD lines for generating submillimeter waves.

4. Experimental characterization of TD lines

4.1 Impulse response

The measured circuit is built on a standard breadboard (Narahara et al., 2008b). The shunt electronic switches are NEC 1S1763 Esaki diodes. The peak current and voltage, which corresponds to V_{pk} in the ideal switch model, are typically 6.0 mA and 60 mV, respectively, and the typical parasitic capacitance is 30.0 pF. Series inductances and shunt capacitances are implemented using 1.0 μH inductors (TDK SP0508) and capacitors (TDK FK24C0G1). To

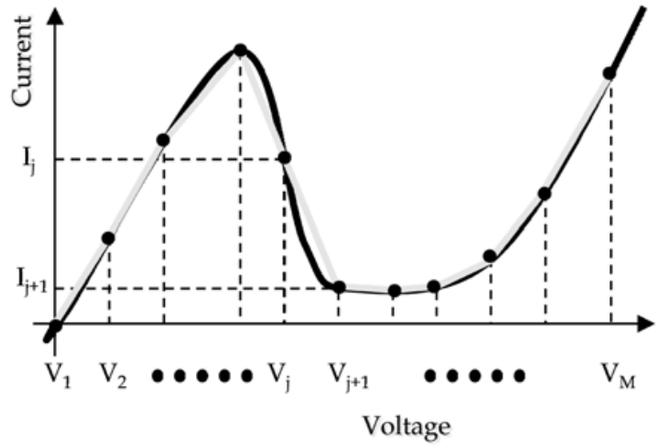

Fig. 8. Piece-wise-linear model of current-voltage relationship of TDs.

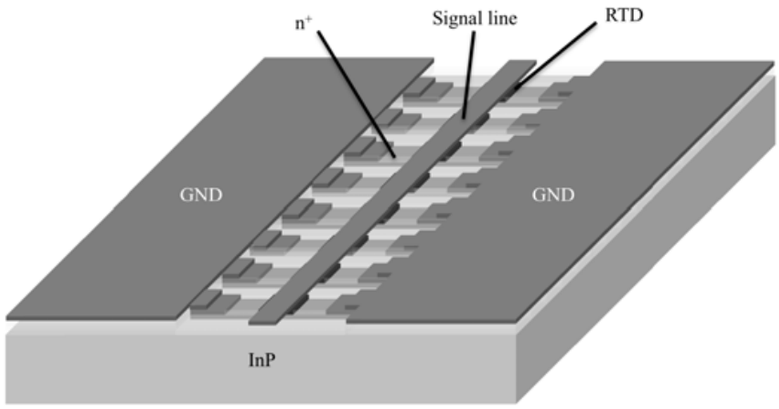

Fig. 9. Line structure used for FDTD test calculation. The signal line is 1.0 mm long, and 30.0 μm wide. The spacing between the signal line and adjacent ground (GND) is set to 30.0 μm. A step pulse is input at the end of the signal line.

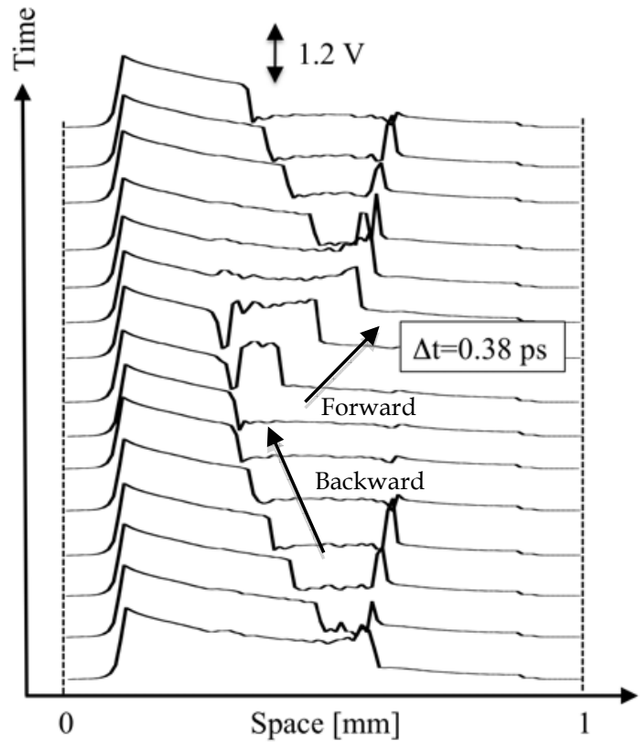

Fig. 10. Results of FDTD calculation.

see the β dependence of the degree of the pulse compression, we prepared two different capacitors, one with a capacitance of 10 nF, and another with 4.7 nF. The test switch line is fed by a pulse signal generated by an Agilent 81150A function generator. The input pulse is a Gaussian pulse with a full-width-at-half-maximum (FWHM) of 1.0 μs. The generator output impedance is set to 5 Ω, and the other end of the test line is short-circuited. The signals along the test switch line are detected and monitored in the time domain using an Agilent DSO90254A oscilloscope.

Figure 11(a) shows the voltage waveforms monitored at cells n=1, 10, 20, 30, 40, and 44. The shunt capacitance is set to 10 nF, such that β=1.0. We can see that the pulse is split in two at n>20. The symbols P_i (i=1, 2, 3, and 4) in Fig.11(a) show the positions of the second pulses developed at n>20. The lifetime of the first pulse is greater than that of the second; therefore, a single short pulse remains at n=44. To determine the degree of compression, we compared the waveform at n=1 (thin solid curve) with that measured at n=44 (thick solid curve) in Fig.11(b). The left vertical axis measures the voltage at n=1, while the right-vertical axis measures the voltage at n=44. Although the amplitude is attenuated, the 1.0-μs wide pulse is compressed to give a width of 0.2 μs after propagation. The attenuated amplitude can result from the parasitic resistances of the inductors and capacitors. It is established that the finite resistive elements do not prevent the switch line from achieving pulse compression.

The results shown in Fig. 12(a) were obtained by the same measurements to obtain those shown in Fig. 11, but with a shunt capacitance of 4.7 nF (β = 1.45). Figure 12(a) shows more compression than seen in Fig. 11(a). This result is consistent with the prediction that a pulse is compressed more for greater β. To quantify the degree of compression, thefundamental

frequency of the resulting single pulse is evaluated. For β=1.0, the fundamental frequency is calculated to be 2.9 MHz, while for β= 1.45, it is 4.2 MHz. This means that the pulse width becomes 70 % smaller for 4.7 nF capacitors than for 10.0 nF over time.Figure 12(b) compares the compressed pulses for both cases. The amplitudes are normalized to make them identical for clear comparison.

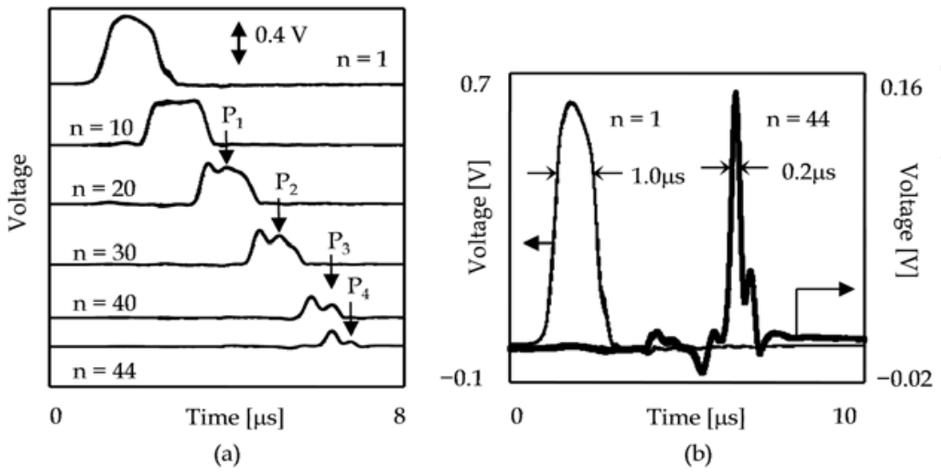

Fig. 11. Measured impulse response of TD line.

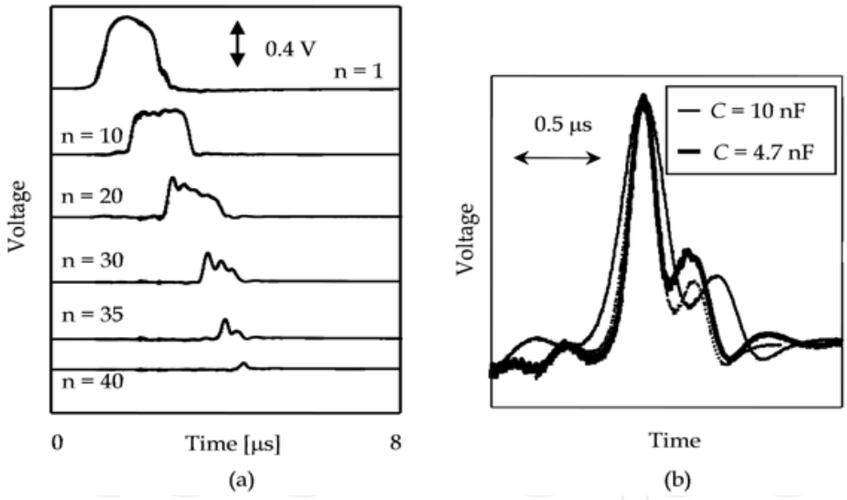

Fig. 12. Measured dependence of shortened pulse width on line capacitance.

The thin and thick pulses represent the compressed pulses for 10.0 and 4.7 nF capacitors, respectively, and the dotted pulse represents the one obtained by artificially compressing the solid pulse by 70 % along the horizontal axis.For the first peak, the dotted pulse fits the thick-solid line well. These observations strongly suggest that the compressed pulses are generated in the test TD line.

4.2 Step pulse response

For step pulse applications, the series inductance, resistance, and shunt capacitance were implemented using 1.0 μH inductors (TDK SP0508), 1.0 Ω resistors (Tyco Electronics

CFR25J), and 470 pF capacitors (TDK FK18C0G1), respectively. To monitor the waveforms using the oscilloscope, we input a pulse having finite duration instead of a step pulse. The input pulse had rise, and fall times, and duration of 1.0 μs, 1.0 μs, and 30.0 μs, respectively. The output impedance of the function generator was 50 Ω.

Figure 13 shows the voltage waveforms monitored at the first cell. Figure 13(a) shows a measured waveform resulting from a single sweep with the oscilloscope. Although the input signal was a simple pulse, we can observe a cycle of short-period pulses. Because of the weakness of the coherence between the input step pulse and the short-period pulses, the temporal positions of the short-period pulses varied for different single sweeps. A typical measured waveform of the short-period pulse is shown in the inset of Fig. 13(a). It exhibits trapezoidal shape with oscillation.

When the pulse edge passes a point, the voltage at that point remains constant until the edge returns. Moreover, the forward edge is carried by the sinusoidal-exponential hybrid mode. These observations are consistent with the measured pulse shape.

Figure 14(a) shows the measured waveform monitored at the first cell, which was averaged 1024 times with the oscilloscope. As mentioned above, the short-period pulses have weak coherence with the step input. Through the waveform averaging, we can extract the coherent part. It is interesting to note that the averaged amplitude of the short-period pulse becomes smaller, i.e., the degree of decoherence increases, with time after the rising edge of

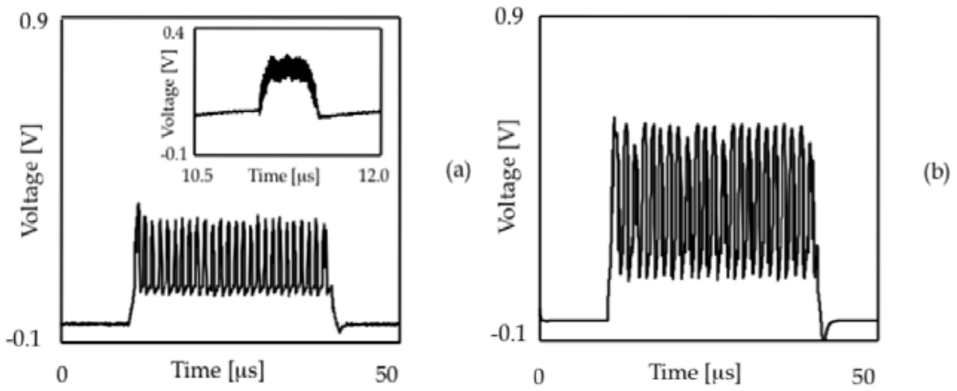

Fig. 13. Experimentally obtained step pulse response of TD line.

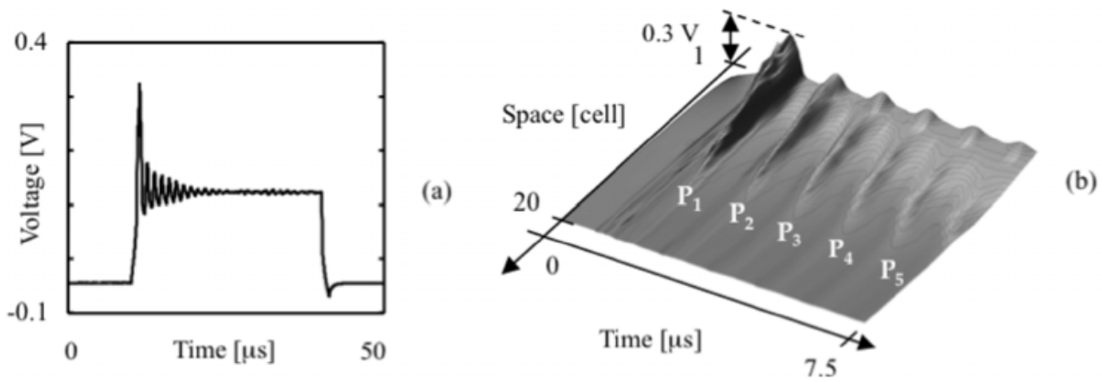

Fig. 14. Observation of oscillating pulse edge.

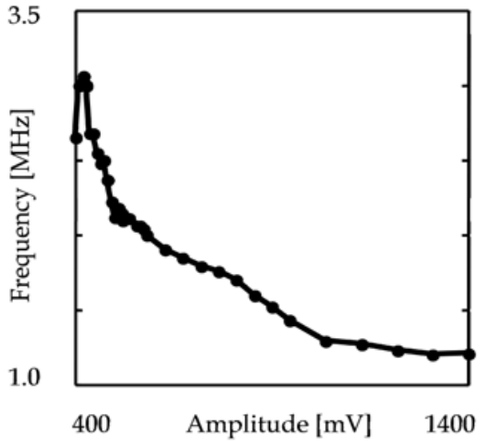

Fig. 15. Measured dependence of edge's oscillating frequency on pulse amplitude.

the input step pulse. By using the coherent parts, it is possible to compare the phase of the voltage waveform at a cell with that at other cells. The spatio-temporal distribution of the averaged voltage wave is shown in Fig. 14(b). The waveforms at the first 20 cells with a 7.5 μs duration are plotted. The edge first travels forward. Then, at the turning point P_i (i=1, 2, 3, 4) in Fig. 14(b), the wave edge starts to travel backward. The backward wave front is reflected at the input port, starts to travel forward again, and reaches the turning point P_{i+1}. This spatio-temporal voltage distribution clearly shows that the oscillating motion of the edge is established in the test switch line.

To examine the dependence of the oscillation frequency on the input amplitude, we carried out frequency-domain measurements, the results of which are shown in Fig.15. We monitored the voltage in the first section using the spectrum analyzer. The frequency of the resulting lowest spectral peak, which corresponds to the inverse of the turn-around time of the oscillating pulse edge, is shown as a function of the input amplitude. Consistently, it is observed that the oscillating frequency increases as the amplitude decreases (Yokota et al., 2009).

5. Applications

This section discusses the potential of TD lines for pulse management. We show two such applications. One is the detection of pulse amplitudes on a one-dimensional TD line. The other utilizes a TD line in two dimensions—the control of pulse propagation orientation on a two-dimensional TD line.

As mentioned above, we consider only pulses that are greater than V_{pk}; therefore, the pulse is attenuated partially at the bottom. It is then expected that a pulse of large amplitude can travel on the line longer than the one with small amplitude. This phenomenon is illustrated in Fig. 16.

Pulses with amplitudes A_1, A_2, and A_3 ($A_1>A_2>A_3$) travel on the TD line by X_1, X_2, and X_3 ($X_1>X_2>X_3$), respectively. When we monitor the waveform at M_1, we detect the pulse regardless of the amplitude. However, because the smallest pulse disappears before it reaches M_2, we can detect only those pulses of amplitudes of A_1 and A_2. Similarly, at M_3, we can detect only the largest pulse. By specifying the monitoring cell on the switch line, we can set thepeak voltage level to detect pulses as required.

Figure 17 shows the measured results. The waveforms were monitored at a fixed cell for two pulses having different amplitudes. By arranging the input amplitudes, only the larger pulse can be detected. Figures 17(a) and (b) show the voltage waveforms monitored at cells n=1 and 5, respectively. The dashed waveforms in Figs. 17(a) and (b) are for the pulse of amplitude 720 mV; the solid waveforms are for the pulse of amplitude 490 mV. Only the dashed pulse is detected at the output. It is thus established that only the larger pulse is detected at the output.

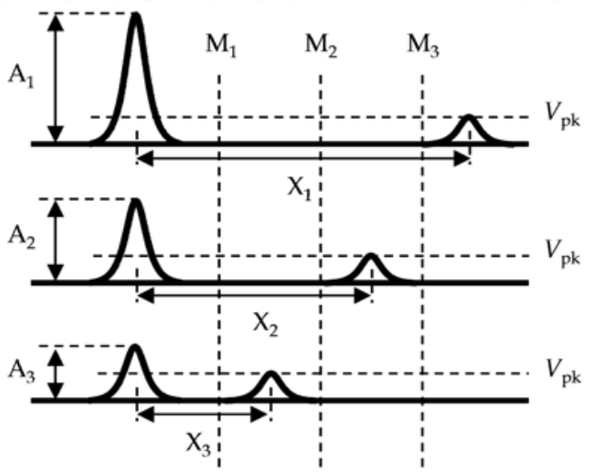

Fig. 16. Pulse control using one-dimensional TD line.

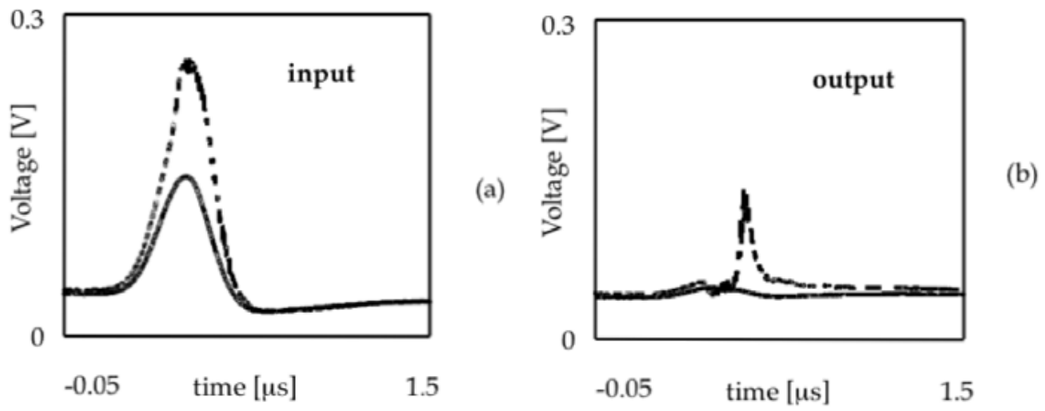

Fig. 17. Experimental demonstration of voltage-level detection.

Another example of the TD line applications requires a two-dimensional TD line. Figure 18 showsa unit cell of two-dimensional TD lines. When several points are excited by the voltage pulses in a two-dimensional line, the propagating pulses overlap and gain amplitude. As mentioned above, the larger pulse survives longer than the smaller pulses; therefore, as time progresses, the overlapped pulses have finite amplitude. The simplest application of this phenomenon is to control pulse propagation orientation by the arrangement of cells where the pulses are applied. To examine the validity of this

application, we numerically solved the transmission line equations of a two-dimensional switch line. We set C, L, V_{pk}, and G_0 as 1.0 pF, 1.0 nH, 0.1 V, and 0.04 S, respectively. The total cell size was 100×100. Each edge cell was terminated using a 50 Ω resistor. An impulse having a Gaussian form with amplitude 1.0 V and FWHM 100.0 ps was input at cells located at (45, 45) and (55, 55).

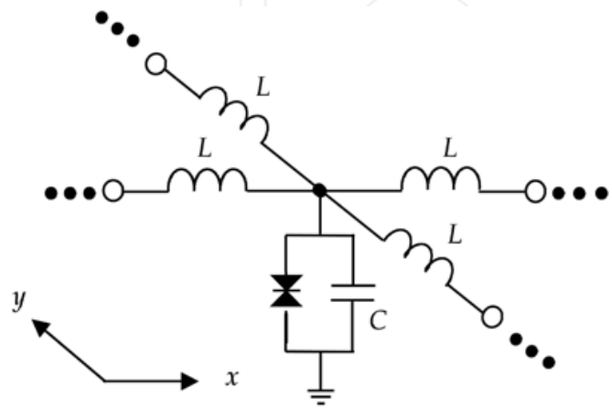

Fig. 18. Two-dimensional TD line.

Figure 19 shows the numerical results of pulse propagation. Waveforms at times 0.4, 0.8, 1.2, and 1.6 ns passed after the pulse incidence are shown in Figs.19(a), (b), (c), and (d), respectively. As observed in Fig. 19(b), each pulse starts isotropic propagation and overlaps the other pulses. As shown in Fig.19(c), the parts of the overlapped pulses with large amplitude survive. The remainders of the pulses on the bisection of the line connecting two excitation cells are shown in Fig.19(d). By changing the positions of the two excitation cells, we can control the propagation orientation of the surviving pulses as required.

For a pulse with a wave vector (k_x, k_y), the dispersions of the two-dimensional switch line are given by

$$v_{I,\sin} = \frac{2}{kd}\sqrt{\sin^2\frac{k_x d}{2} + \sin^2\frac{k_y d}{2}}, \tag{15}$$

$$v_{II,\exp} = -\frac{\beta}{2kd} + \frac{1}{2kd}\sqrt{\beta^2 + 16\sinh^2\frac{k_x d}{2} + 16\sinh^2\frac{k_y d}{2}}, \tag{16}$$

where $v_{I,\sin}$, and $v_{II,\exp}$ show the normalized phase velocities of the sinusoidal mode in region I, and the exponential mode in region II, respectively. Because the cutoff frequency increases monotonically with $\theta = \tan^{-1}(k_x / k_y)$ up to $\pi/4$ and is $\sqrt{2}$ times as large as at $\theta = 0$, it becomes possible for the intersection frequency, where $v_{I,\sin}$is coincident with $v_{II,\exp}$, in a two-dimensional switch line to surpass the upper limit achieved in a one-dimensional switch line; therefore, we can expect that the pulse shortening is more effectively established in two dimensions.

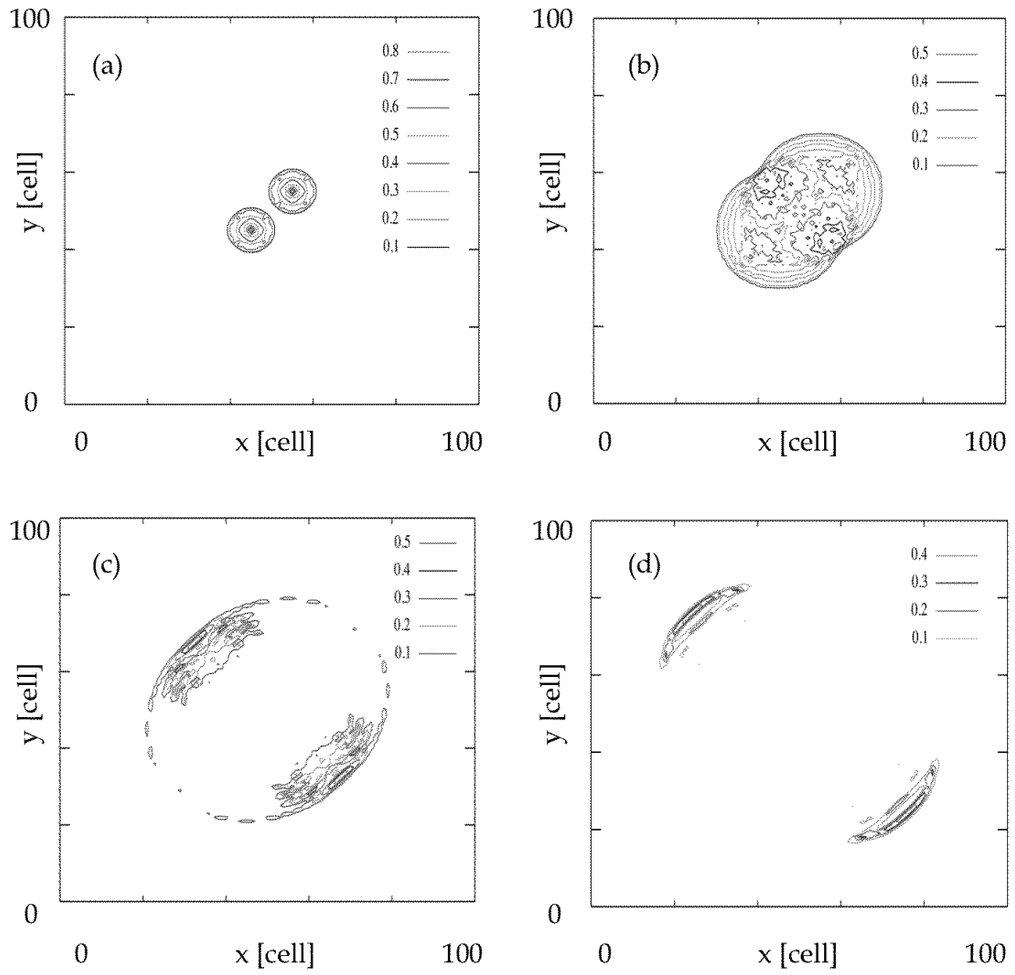

Fig. 19. Fundamental property of two-dimensional TD line.

6. Conclusions

This chapter reviews the pulse propagation characteristics of TD lines.We found that a pulse wave propagates on the line either by theunstable exponential-sinusoidal hybrid mode or stable exponential-exponential mode. Through thesepeculiar wave propagation properties, an input impulse experiences width shortening and an edge of the step pulse oscillates. These provide efficient methods for generating short pulses and continuous waves. Moreover, TD lines can be used to manage pulse amplitude and propagation orientation. Test TD lines using Esaki diodes successfully demonstrated the pulse generation and management.Our approach could be scaled from its current MHz form into microwave, millimeter-wave, and terahertz forms, for implementation with state-of-the-art RTDs.

7. References

Brown, E.R.; Soderstrom, J.R.;Parker, C.D.; Mahoney, L.J.; Molvar, K.M. &McGill, T.C. (1991). Oscillations up to 712 GHz in InAs/AlSb resonant-tunneling diodes, Applied Physics Letters, Vol.58, 2291-2293, ISSN:0003-6951.

Kintis, M.; Xing, L.; Flavia, F.; Sawdai, D.; Kwok, L.K. &Gutierres, A. (2008). An MMIC pulse generator using dual nonlinear transmission lines, Microwave and Wireless Components Letterts, Vol.17, No.6, 454-457, ISSN: 1531-1309.

Luebbers, R.; Beggs, J. & Chamberlin, L. (1993). Finite difference time domain calculation of transients in antennas with nonlinear loads, IEEE Transacions on Antennas and Propagation, Vol.41, No.5, 566-573, ISSN:0018-926X.

Narahara, K.; Otsuji, T. &Sano, E. (2006). Pulse compression by quasi-steady propagation along switch lines, Japanese Journal of Applied Physics, Vol.45, No.7, 5692-5695, ISSN: 0021-4922.

Narahara, K.; Otsuji, T. &Sano, E.(2006). Generation of electrical-short-pulse using Schottky line periodically loaded with electronic switches, Journal of Applied Physics, Vol.100, No.2, 024511.1-5, ISSN: 0021-8979.

Narahara, K. (2006). Electromagnetic continuous-wave generation using switch lines, Journal of Applied Physics, Vol.100, No.6, 064908.1-5, ISSN: 0021-8979.

Narahara, K. & Yokota, A. (2008a). Full-wave analysis of quasi-steady propagation along transmission lines periodically loaded with resonant tunneling diodes, Japanese Journal of Applied Physics, Vol.47, No.2, 1126-1129, ISSN: 0021-4922.

Narahara, K. & Yokota, A. (2008b). Experimental characterization of short-pulse generation using switch lines, IEICE Electronics Express, Vol.5, No.22, 973-977, ISSN: 1349-2543.

Ohashi, N.; Hattori, S.; Suzuki, S. &Asada, M. (2005). Experimental and theoretical characteristics of sub-terahertz and terahertz oscillations of resonant tunneling diodes integrated with slot antennas, Japanese Journal of Applied Physics, Vol.44, No.11, 7809-7815, ISSN: 0021-4922.

Richer, I. (1966). The switch-line: A simple lumped transmission line that can support unattenuated propagation. IEEE Transactions on Circuit Theory, Vol.13, No.4, 388-392, ISSN: 0018-9324.

Rodwell, M.J.W.; Allen, S.T.; Yu, R.Y.; Case, M.G.; Bhattacharya, U.; Reddy, M.; Carman, E.; Kamegawa, M.; Konishi, Y.; Pusl,J. &Pullela, R. (1994). Active and nonlinear wave propagation devices in ultrafastelectronics and optoelectronics, Proceeding of the IEEE, Vol.82, No.7, 1037-1059, ISSN: 0018-9219.

Scott, A. (1970). *Active and nonlinear wave propagation in electronics*, Wiley-Interscience, ISBN: 471767905 New York.

Sugiyama, H.; Matsuzaki, H.; Oda, Y. & Yokoyama, H. (2005). Metal-organic vapor-phase epitaxy growth of InP-based resonant tunneling diodes with a strained $In_{0.8}Ga_{0.2}As$ well and AlAs barriers, Japanese Journal of Applied Physics, Vol.44, No.10, 7314-7318, ISSN: 0021-4922.

Taflove, A. (1995). *Computational electrodynamics: the finite-difference time-domain method*, Artech House, ISBN: 1580538320,London.

Yee, K.S. (1966). Numerical solution of initial boundary value problems involving Maxwell's equations in isotropic media, IEEE Transactions on Antennas and Propagation, Vol.14, No.4, 302-307, ISSN:0018-926X.

Yokota, A. &Narahara, K. (2009). Characterization of oscillating pulse edges in switch lines for development of widely tunable voltage-controlled oscillators, Japanese Journal of Applied Physics, Vol.48, No.8, 084502-084506, ISSN: 0021-4922.

Wave Propagation in Materials for Modern Applications

Edited by Andrey Petrin

ISBN 978-953-7619-65-7
Hard cover, 526 pages
Publisher InTech
Published online 01, January, 2010
Published in print edition January, 2010

In the recent decades, there has been a growing interest in micro- and nanotechnology. The advances in nanotechnology give rise to new applications and new types of materials with unique electromagnetic and mechanical properties. This book is devoted to the modern methods in electrodynamics and acoustics, which have been developed to describe wave propagation in these modern materials and nanodevices. The book consists of original works of leading scientists in the field of wave propagation who produced new theoretical and experimental methods in the research field and obtained new and important results. The first part of the book consists of chapters with general mathematical methods and approaches to the problem of wave propagation. A special attention is attracted to the advanced numerical methods fruitfully applied in the field of wave propagation. The second part of the book is devoted to the problems of wave propagation in newly developed metamaterials, micro- and nanostructures and porous media. In this part the interested reader will find important and fundamental results on electromagnetic wave propagation in media with negative refraction index and electromagnetic imaging in devices based on the materials. The third part of the book is devoted to the problems of wave propagation in elastic and piezoelectric media. In the fourth part, the works on the problems of wave propagation in plasma are collected. The fifth, sixth and seventh parts are devoted to the problems of wave propagation in media with chemical reactions, in nonlinear and disperse media, respectively. And finally, in the eighth part of the book some experimental methods in wave propagations are considered. It is necessary to emphasize that this book is not a textbook. It is important that the results combined in it are taken “from the desks of researchers“. Therefore, I am sure that in this book the interested and actively working readers (scientists, engineers and students) will find many interesting results and new ideas.

INTECH
open science | open minds

InTech Europe
University Campus STeP Ri

InTech China
Unit 405, Office Block, Hotel Equatorial Shanghai

www.intechopen.com

Slavka Krautzeka 83/A
51000 Rijeka, Croatia
Phone: +385 (51) 770 447
Fax: +385 (51) 686 166
www.intechopen.com

No.65, Yan An Road (West), Shanghai, 200040, China
中国上海市延安西路65号上海国际贵都大饭店办公楼405单元
Phone: +86-21-62489820
Fax: +86-21-62489821

IntechOpen

IntechOpen